Materials Today Bio 16 (2022) 100421

Contents lists available at ScienceDirect

Materials Today Bio

journal homepage: www.journals.elsevier.com/materials-today-bio

Nanozyme-laden intelligent macrophage EXPRESS amplifying cancer photothermal-starvation therapy by responsive stimulation

Yan Zhang [a,1], Kunpeng Wang [b,1], Guozheng Xing [a], Xia Dong [a,**], Dunwan Zhu [a], Wenzhi Yang [b,***], Lin Mei [a], Feng Lv [a,*]

[a] Tianjin Key Laboratory of Biomedical Materials, Key Laboratory of Biomaterials and Nanotechnology for Cancer Immunotherapy, Institute of Biomedical Engineering, Chinese Academy of Medical Sciences & Peking Union Medical College, Tianjin 300192, PR China

[b] College of Pharmacy & Key Laboratory of Pharmaceutical Quality Control of Hebei Province, Hebei University, Baoding 071002, PR China

ARTICLE INFO

Keywords:
Nanozyme
Macrophages express
Precise delivery
Cancer photothermal-starvation therapy
Environment-responsiveness

ABSTRACT

Precise delivery and responsive activation of therapeutic agents are critical for tumor precise therapy. Herein, inspired by intelligent express, a nanozyme-laden intelligent macrophage express was fabricated based on IR 820-macrophage loaded with GOx nanozymes for tumor-targeted photothermal-amplified starvation therapy with fluorescence imaging guidance. The nanozyme-laden intelligent macrophage express exerted precise delivery through cargo loading, conveying and unloading. For efficient cargo loading, H_2O_2-sensitive GOx nanozymes with blocked enzymatic activity were packaged on macrophage expresses with excellent phagocytic ability. Due to the inherent tumor tropism, the therapeutic agents-laden macrophage expresses naturally accumulated at tumor site with fluorescence navigation to track the conveying process. The spatiotemporal unpacking of the laden therapeutic agents at tumor site was triggered by the external laser for the macrophage express photothermal property. The released special tumor-microenvironment responsive GOx nanozymes were activated by H_2O_2 in tumor to start starvation therapy. Photothermal therapy generated mild hyperthermia and starvation therapy produced H_2O_2 further increased the nanozymes enzymatic activity, enhancing GOx-mediated starvation therapy. The nanozyme-laden intelligent macrophage express integrated laser-induce drug release and activation, tumor microenvironment-responsiveness, and circular amplification property, achieving the synergistic effects of PTT and starvation therapy *in vitro* and *in vivo*.

1. Introduction

Tumor has abnormal cell metabolic behavior with addictive consumption of glucose to maintain its excessive cell proliferation [1–3]. Over the decades, different approaches targeting abnormal metabolism have received increasing attention in tumor therapy [3], such as cancer starvation therapy (CST) by blocking essential nutrients and energy [4,5]. Glucose oxidase (GOx) could effective convert glucose and oxygen into toxic hydrogen peroxide (H_2O_2) and gluconic acid, depleting glucose in microenvironment [6]. So GOx-mediated starvation therapy has been emerged as an attractive strategy against tumor by cutting off indispensable nutrient supply to inhibit tumor proliferation [6,7]. However, GOx-mediated starvation therapy faced challenges as enzymatic inactivation due to exposure to biological conditions, and potential toxic effects of off-target GOx [8,9]. To overcome these problems, transformation of GOx into tumor environment-responsive nanozyme with high stability and tunable activity is an effective strategy [10,11]. Abnormality of tumor metabolism generates the specific tumor microenvironments (TME), including low pH [12], and high level of reactive oxygen species (ROS) [13]. H_2O_2 as a hallmark is over produced in TME and tumor cytoplasm, providing a pathway for selective and efficient activation of GOx nanozymes [14]. Therefore, the construction of H_2O_2-responsive GOx nanozyme could exert the controllable release and activation of GOx as a step for efficient cancer starvation therapy.

Notably, how to precisely deliver nanozyme to targeted tumor site is a key issue to consider. Targeted delivery with imaging navigation is an

* Corresponding author. Institute of Biomedical Engineering, Chinese Academy of Medical Sciences & Peking Union Medical College, Tianjin 300192, PR China.
** Corresponding author. Institute of Biomedical Engineering, Chinese Academy of Medical Sciences & Peking Union Medical College, Tianjin 300192, PR China.
*** Corresponding author.
E-mail addresses: dongxiatj@163.com (X. Dong), wenzhi_yang@sina.com (W. Yang), lvfeng2002@163.com (F. Lv).
[1] These authors contributed equally as co-first authors.

https://doi.org/10.1016/j.mtbio.2022.100421
Received 21 July 2022; Received in revised form 2 September 2022; Accepted 3 September 2022
Available online 6 September 2022

effective strategy for precise tumor delivery that we have recently developed [15,16]. Macrophage-based drug delivery system has attracted intensive attention for its unique characterizations as biocompatibility, phagocytic property, vessel migration and tumor infiltration [17–19]. Attributed to the inherent tumor tropism, macrophage-based delivery system could naturally target therapeutic drugs to tumor site [19,20]. Previous studies have reported a series of macrophage delivery systems engulfed Dox, nanozymes or liposomes, which appeared good therapeutic effects by targeted delivery [21,22]. Another concern for precise delivery is the imaging tracking of delivery process *in vivo* to enable visual guidance for tumor treatment. Fluorescence imaging has been introduced into imaging-guided drug delivery for its high sensitivity and non-destructiveness [23,24]. Integrating fluorescence navigation into the cell-based delivery system could provide real-time information to guide treatment timing and dosing cycle for precise delivery on-demand. Our previous work has reported fluorescence imaging-guided chemotherapy, immunotherapy, or thermal therapy with favorable efficiency [15,25]. Especially, we have constructed IR-820 modified macrophage to achieve the fluorescence imaging-guided tumor therapy by precise delivery [16]. Based on these, we plan to further carry out functional macrophages-based delivery system for precise delivery of nanozymes in order to achieve better cancer starvation therapy.

The final step in achieving precision therapy is to promote the activation of nanozymes through controlled stimulation. The responsive drug release could be controlled by different physical, chemical, or biological stimuli either internal or external [26,27]. Given the high spatiotemporal controllability, deep penetration ability and beneficial photothermal effect, near infrared (NIR) laser is an impressive trigger for localized release and activation [21,28,29]. For the cancer starvation therapy of nanozymes, near infrared photothermal control of their focused and timely release in tumor can effectively reduce the toxicity and promote the catalytic effect of nanozymes [30,31]. Furthermore, NIR laser induced photosensitizers to generate localized hyperthermia from light energy, exhibiting high specific treatment for thermal ablation of tumor tissue and nearby cells [21,32]. Thus, NIR fluorescent photosensitizer modified system can play the dual role of photo-controlled drug release and photothermal therapy simultaneously. Tumor starvation therapy and photothermal therapy could promote and complement each other to achieve better combined treatment effect [31,33]. A series of nanoscale nanozymes, like hollow prussian blue nanoparticles loaded GOx nanosized biocatalyst [30], heptamethine cyanine dye (Cy7)-conjugated GOx nanoagents [33], GOx and tirapazamine co-loaded polydopamine doped poly(vinyl alcohol) microbubble [34], and GOx-conjugated polyaniline nanoplatform [35], have been reported to achieve combined tumor starvation and photothermal therapy. The GOx-mediated CST can block energy supply to tumor cells, which is beneficial to promote the PTT efficacy in mild temperature, whereas the enzymatic activity of GOx varies with temperature, and exhibits the optimal catalytic properties under PTT at local tumor. Therefore, the combination of PTT and GOx–mediated starvation therapy was a win-win cooperation, achieving superior combinational therapeutic efficacy with controllable release and activation.

In this regard, inspired by intelligent express, a nanozyme-laden intelligent macrophage express based on IR 820-macrophage loaded with GOx nanozyme was constructed for tumor synergetic photothermal-activated starvation therapy (Fig. 1). The nanozyme-laden intelligent macrophage express divided three steps including cargo loading, conveying and unloading. Firstly, the packing process was achieved for the excellent phagocytic ability of macrophages. To reduce damage to the host cells, high active GOx was fabricated into H_2O_2-sensitive nanozymes (GNPs) with high stability for specific environment responsive activation. Multifunctional therapeutic macrophage express (IRG@RC) was constructed with encapsulation of therapeutic agent GNPs and fluorescent photosensitizer IR-820. This construction of macrophage express could achieve large amount of drug encapsulation with maintained host cell viability, as well as the protect the activity of GNPs from degradation in the physiological environment before reaching the tumor site. Secondly, based on the inherent tumor tropism, IRG@RC could be accumulated in tumor site. With fluorescence navigation, this conveying process could be monitored, realizing the targeted and precise delivery with imaging guidance. Finally, the spatiotemporal unpacking process of the laden therapeutic agents at tumor site was triggered by the external laser and the special tumor microenvironment, amplifying cancer photothermal-starvation therapy by responsive stimulation. Exposed to external laser, the IRG@RC express was destroyed to release encapsulated H_2O_2-sensitive GNPs, and subsequently GNPs were activated by the high H_2O_2 level in tumor, inducing glucose consumption to initial starvation therapy. Of note, the generated H_2O_2 in CST was a positive feedback microenvironment, and conversely attacked the H_2O_2-sensitive shell of GNPs, further enhancing their activation. Moreover, laser-triggered PTT could generate hyperthermia in tumor site, inducing the tumor apoptosis, accelerating the decomposition of H_2O_2 into O_2 [36], and enhancing the GOx enzyme activity for starvation therapy. The

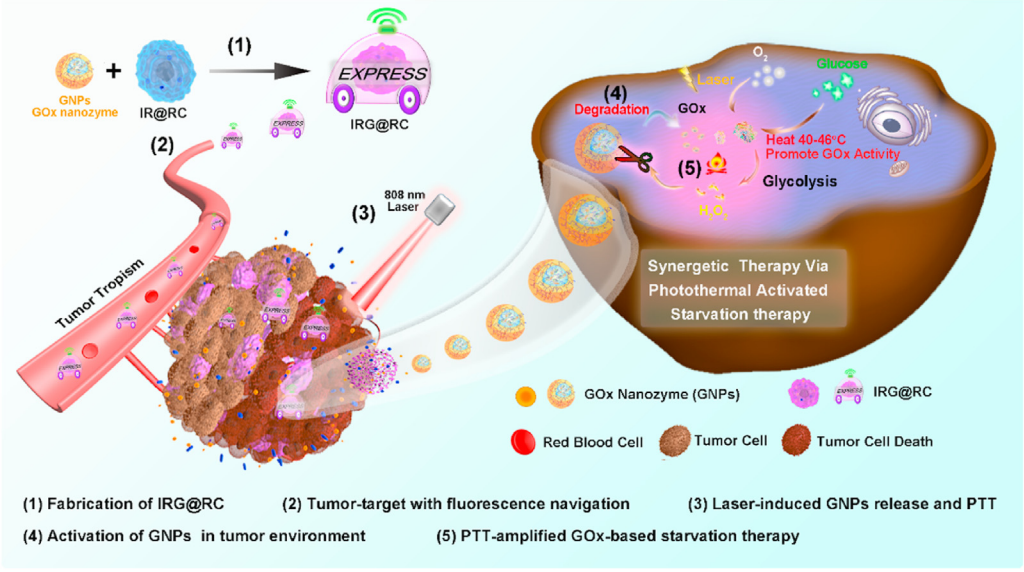

Fig. 1. Scheme of the functional therapeutic macrophage expresses for PTT-amplified starvation therapy. (1) Functional therapeutic macrophage expresses were constructed based on IR 820-macrophage (IR@RC) loaded with GOx nanozyme (GNPs). (2) Fluorescence imaging tracking conveying process of IRG@RC expresses after intravenous injection: targeted delivery therapeutic agents to tumor site by the inherent tumor tropism. (3) Laser induced the fracture of IRG@RC expresses to release packaged GNPs and PTT therapy. (4) High intracellular H_2O_2 induced the activation of GNPs to trigger starvation therapy. (5) PTT induced mild temperature and generated H_2O_2 amplified the starvation therapy.

nanozyme-laden intelligent macrophage express integrated the multi-functions as real-time imaging, targeted drug delivery, spatiotemporal release and activation of nanozyme, and the synergetic tumor therapy. It could be speculated that the efficient tumor outcomes could be achieved with PTT-amplified starvation therapy under fluorescence imaging guidance.

2. Material and methods

2.1. Fabrication and characterization of H_2O_2-responsive GOx/PEI nanozymes (GNPs)

The H_2O_2-responsive nanozymes GNPs were prepared by linking GOx and PEI via H_2O_2-sensitive crosslinkers. The GOx solution (5 mg/mL) was mixed with PEI at 10 mg/mL to stir for 1 h. The subsequent addition of the H_2O_2-responsive compound PDAA which was pre-prepared as an active ester by EDC and NHS activation to initiate the cross-linking reaction. After stirring for 6 h, the ensemble solution was dialyzed for 48 h and lyophilized to obtain the GNPs.

The GOx could catalyze the conversion of glucose to generate the H_2O_2 and gluconic acid, reducing the pH value. For measuring the catalytic activity of the GOx in the H_2O_2-sensitive nanozymes, the real time pH of the solution was monitored using a pH meter (PHS-25 pH Meter, INESA Scientific, China). To evaluate the temperature dependence of nanozyme, GNPs was mixture with glucose (1 mg/mL) in a water at different temperature (25, 37, or 42 °C) with stirring. To assess the H_2O_2-responsiveness, GNPs was mixed with reaction solution, which containing 1 mg/mL glucose and different concentration of H_2O_2 (0, 1, 5, or 10 mM). The change in H^+ concentration was calculated according to the following equation:

$$\Delta \text{ Concentration } (H^+) = 10^{-pH(final)} - 10^{-pH(initial)}$$

where pH (final) and pH (initial) represent the pH values at the detection and initial time point, respectively.

To determine the disassemble of GNPs in responsive to H_2O_2 environment, GNPs were added with saline, 0.03% H_2O_2 medium, or 0.3% H_2O_2 medium, respectively, and the final concentration was 0.5 mg/mL. After 5 min, 1, 2 or 4 h incubation at room temperature, the samples were tested for intensity particle size on a Malvern instrument (Zetasizer Nano ZS 90). The size change of GNPs in glucose was also recorded after incubated with 1 mg/mL glucose for 1 h.

2.2. Fabrication and characterization of multifunctional macrophages-based express

The photothermal agent IR-820 decorated RAW 264.7 cell expresses (IR@RC) were fabricated by conjugated the IR-NHS with the proteins in cytoplasm in our previous paper [16]. The GOx loaded therapeutic expresses (G@RC or IRG@RC) were prepared by rhodamine-labelled GNPs incubation. The macrophages were incubated with nanozymes at different concentration. Then the intracellular rhodamine fluorescent intensity was analyzed by flow cytometer (FACS Calibur, BD, America), and the intracellular GOx amount was evaluated by fluorescent spectroscopic analysis (FluoroMAX-4C-L, HORIBA Scientific, America). For directly visualize distribution of GNPs, the IRG@RC cells were stained with Hoechst 33342 to identify the nuclei location, and then fluorescence images were recorded on a confocal laser scanning microscope (ZEISS LSM 710, Germany). The *ex vivo* release profile of GOx NPs from G@RC or IRG@RC was accessed by measuring the rhodamine signal in the supernatant using fluorescence spectroscopy.

The impact of the intracellular GOx on the macrophage-based expresses was evaluated by the MTS assay. The cells were incubated with GNPs in different GOx concentration for 2 h, and then the glucose-free medium was replaced with complete culture with incubation for another 22 h. The cell cytotoxicity of the GOx were related with the conversion of glucose into H_2O_2 and glutamic acid, so the cell viability of G@RC was also studied in culture medium with different glucose concentration.

To verify the photothermal effect of IR@RC and IRG@RC expresses, solution of dispersed expresses was illuminated by a near-infrared light laser (808 nm, 1 W/cm^2) for 5 min, and the thermal imaging was taken by an infrared thermal imaging camera (E6, FLIR System Inc, America) to record the temperature every minute. To assess the fluorescence navigation, the *in vitro* fluorescence imaging of IR@RC and IRG@RC expresses was taken on the *in vivo* imaging system (Maestro EX, CRI, America) with laser irradiation or not.

2.3. In vitro tumor microenvironment modulated by the IRG@RC expresses

Firstly, the transfer of therapeutic agents between macrophage expresses and tumor cells was evaluated. 4T1 cells, preincubated for 24 h, were cocultured with IRG@RC express with laser trigger to control the release of loaded GNPs from express. After 24 h incubation, the fluorescence imaging was taken by confocal laser scanning microscope (LSM 710, ZEISS, Germany).

Then the intracellular H_2O_2 and pH value were detected by BES–H_2O_2–Ac probe and pH probe BCECF-AM, respectively. 4T1 cells were seeded into 6-well plates at a density of 2×10^5 cells per well and incubated for 24 h. The medium was placed with fresh 1640 containing PBS, GNPs, and IRG@RC express (The GOx concentration was 0.2 μg/mL) for another 24hr. For wells treated with IRG@RC expresses, cells were exposed to 808 nm laser to control the GNPs release. The medium was removed and fresh medium containing 30 μmol/L BES- H_2O_2–Ac probe or 10 μmol/L BCECF-AM probe for 1 h, respectively. Then the cells were washed with PBS, collected by trypsin, and the fluorescence was analyzed by flow cytometry.

2.4. In vitro 4T1 tumor cells inhibition of multifunctional macrophages-based expresses

4T1 tumor cells inhibition by macrophages expresses (IR@RC, GNP@RCT, or IRG@RC) was studied. CFSE-tagged 4T1 cells (4.0×10^5) were suspended with expresses (1.0×10^5 or 2.0×10^5) in RPMI medium. The groups incubated with IR@RC or IRG@RC expresses were irradiated by 808 nm laser irradiation at a power density of 1.0 W/cm^2 for 0, 30, or 60 s. Then the mixture cells were incubated for 24 h, and subsequently washed with PBS and stained with propidium iodide (PI). To evaluate the cell viability, the PI-stained cells as death were counted by flow cytometry.

2.5. Tumor microenvironment assessment in vivo

When the tumor size reached 100 mm^3, the 4T1 tumor bearing mice were divided into five groups with intratumor injection of saline, GOx NPs (GNPs), or IRG@RC express, respectively. Note that part of the mice injected with IRG@RC express were exposed to laser at 12 h post injection. After 24 h, the mice were sacrificed and tumors were collected and homogenized to produce single cell suspension. The intracellular environment of H_2O_2 was measured using the hydrogen peroxide content detection kit. To assess intracellular pH, cells were stained with pH probe BCECF-AM for 30 min at 4 °C, and then intracellular green fluorescence of BCECF was analyzed by flow cytometry. To examine the glucose consumption, tumor cells were incubated with 2-[N-(7-nitrobenz-2-oxa-1,3-diazol-4-yl) amino]-2-deoxy-d-glucose (2-NBDG) for 30 min in the dark at 4 °C, and the intracellular 2-NBDG fluorescence was analyzed by the flow cytometry.

2.6. Tumor retention of multifunctional expresses and in vivo photothermal imaging

To access the tumor retention of the therapeutic expresses, 4T1

tumor-bearing mice were intravenously injected with saline, IR-stained GOx NPs (IRG NPs), IR@RC express, or IRG@RC express at an equivalent IR-820 dose (1 mg/kg) respectively. Then the fluorescence imaging on tumor region in mice was recorded daily by *in vivo* imaging system. The external laser at a power density of 1.0 W/cm^2 was added at 1st and 4th day. Fluorescence images of each sample were analyzed. The relative fluorescence intensity of tumor was calculated by comparing with the fluorescence intensity at 1st day. When the tumor sites were exposed to the external, the temperature variation at tumor was depicted by infrared thermal imaging camera every minute.

2.7. Tumor growth inhibition

The 4T1-Luc tumor bearing mice were divided into five groups with i.v. injection as follow: (1) saline as control, (2) IRG NPs, (3) IR@RC express, (4) and (5) IRG@RC express. The dose of IR or GOx was 1 mg/kg and 3 mg/kg respectively, and the group (2), (3) and (5) were expose to 808 nm laser at day 1 and 4 after injection, and the laser density was 1.0 W/cm^2 for 5 min. Tumor size and body weight were recorded every other day in following 20 days. Meanwhile, the tumor volume was also monitored for each 5-day period by bioluminescence imaging (IVIS Lumina system, Xenogen, America). In the end, mice were sacrificed and tumor were collected and weighted. The resected tumor tissue was fixed and stained with hematoxylin and eosin (H&E) for histology analysis. The paraffin-embedded tumor slices were deparaffinized and rehydrated for immunofluorescence-stain with PCNA, Ki67 antibody and immunofluorescence Detection Kit, and TUNEL assay kit according to the manufacturer's instruction.

3. Results and discussion

3.1. Fabrication and characterization of GNPs

For a cell-based express, it was essential to balance the drug loading capacity and drug toxicity to host cells. GOx could directly catalyze the conversion of glucose into H_2O_2 and gluconic acid, reducing the environment pH to cause toxicity. To escape the direct toxicity of GOx to host express, it was a feasible strategy to shield GOx in nanozymes to reduce its catalytic activity. Meanwhile, the activation of the shielded GOx in tumor targets was a key issue that needs to be taken into consideration to achieve efficient tumor treatment. The abnormal tumor metabolism induced the higher level of H_2O_2 in tumor tissues (20–100 $\times$ 10^{-6} M) than that in normal physiology (~0.1 $\times$ 10^{-6} M), ensuring H_2O_2 as a cancer–associated stimulus for controlled drug release [14,37]. Herein, the H_2O_2-responsive nanozymes GNPs were prepared by linking GOx and PEI via H_2O_2-sensitive crosslinker PDAA (Fig. 2 a). Notably, H_2O_2-sensitive shell could ensure GOx stability and hide its catalytic ability to alleviate safety concerns in host macrophages. The H_2O_2 in TME could trigger the activation of GNPs, inducing the glucose oxidation to initial starvation therapy. In addition, the generated H_2O_2 during the GNPs catalytic process could further amplify the H_2O_2 responsiveness of GNPs. TEM image (Fig. 2 b) revealed that the GNPs displayed the spherical structures, and the average hydrodynamic diameter (Fig. 2 c) was 166.7 $\pm$ 13.25 nm. The zeta potential changed from $-$20.3 $\pm$ 2.61 mV for free GOx to 22.6 $\pm$ 3.73 mV for GNPs due to the positive charged PEI polymer shell, which was beneficial to phagocytosis of nanozymes to achieve efficient loading. (Fig. 2 d). UV–Vis spectra (Fig. S1) of GOx and GNPs were recorded to evaluate the GOx content in the GNPs. The loading capacity of GOx was 0.075 mg/mg and the loading efficiency was 82.6%, which was determined by the UV–Vis absorption at 278 nm.

GNPs could effectively deplete glucose in the presence of O_2 to generate gluconic acid and H_2O_2, thereby inducing a decrease of pH. The newly generated H_2O_2 could decompose H_2O_2-responsive linker to expose the GOx, enhancing the glucose consumption rate (Fig. 2e). The catalytic property of GNPs was measured by monitoring the change of H^+ concentration (ΔH^+). As shown in Fig. 2g, the H^+ concentration increased slowly in the first 5 min and then gradually increased with time. When the H_2O_2 was added to the GNPs/glucose system, a rapid increase in H^+ concentration could be observed, and the increase of H^+ concentration was dependent on H_2O_2 concentration. It could be rationalized that added or generated H_2O_2 could decompose H_2O_2-responsive PDAA linker to expose the shielded GOx in GNPs, enhancing the production of gluconic acid and H^+. To elucidate the decomposition of GNPs in responsive to H_2O_2 environment, the change of GNPs size was monitored by DLS. Data in Fig. S2 demonstrated the size change with time dependence. The particles sizes of GNPs keep unchanged in saline and decompose into particles with various size in H_2O_2 medium. In addition, the intensity-magnitude frequency curve shows multiple peaks in GNPs incubated in glucose solution for 1 h (Fig. S3). Furthermore, the effect of the temperature on ΔH^+ was also studied. The data in Fig. 2 f displayed the temperature dependence of GNPs catalytic activity. At room temperature of 25 °C, the generated H^+ in 20 min was ~11 μM, while the value of ΔH^+ increased to ~35 μM at 37 °C. As the temperature continues to rise, the ΔH^+ reached ~128 μM at 42 °C, which was 11.5 and 3.6 times than that at 25 and 37 °C, respectively. Of note, it could be observed the gap of ΔH^+ between 37 °C and 42 °C were significantly widened with time, suggesting the generated H_2O_2 was in turn to further activate the GNPs. It could be speculated that the mild hyperthermia at tumor region could enhance the activity of GNPs locally released by NIR laser. This kind of enhanced catalytic activity of GNPs with temperature was beneficial for tumor photothermal-amplified starvation therapy.

3.2. Preparation and characterization of therapeutic macrophages express

Based on the IR-820 modified macrophage to achieve the fluorescence imaging guided tumor therapy by precise delivery [16], we further carried out functional macrophages-based delivery system for precise delivery of nanozymes in order to achieve better cancer starvation therapy. The package of therapeutic agents with large amount was an important prerequisite for constructing a cell-based express with ideal therapeutic outcomes. Macrophages could naturally carry micro- to nano-scale therapeutic vectors via cellular endocytic pathway [38], so a sufficient amount of nanozymes could be easily packaged in macrophages-based expresses. In order to pack the nanozyme into macrophage expresses, we need to suppress its toxicity to maintain the express vitality. The harm of GNPs to macrophages was first assess by MTS assay. In the absence of glucose, the GNPs was benign towards the macrophages (Fig. 3a), and the cell viability was higher than 80% even incubated with 10 μg/mL GOx. The GOx-induced cell death was due to the glucose consumption and H_2O_2 generation, then the viability of GNPs packed macrophage expresses was further assessed in medium with different glucose concentration. The decrease of cell viability could be noticed with the increase of the glucose concentration (Fig. 3b), suggesting the trigger of GOx-based starvation therapy by glucose medium in macrophages expresses. Considering glucose concentration in blood is between 70 and 140 mg/L [39], the viability of GNPs-packed macrophage expresses was over 70% at medium containing 2.25 mg/mL glucose, thus acceptable vitality of express was maintained to achieve efficient tumor target.

To determine the GOx encapsulation efficacy, the macrophages were incubated with GNPs in different condition to determine the intracellular GNPs by flow cytometry (Fig. 3c and Fig. S4). The GNPs laden behavior by macrophage expresses demonstrated the time and concentration dependence. Then the intracellular GOx amount was quantitatively analyzed by fluorescence spectra. When incubated with GNPs at 2.5 μg/mL for 1, 2, or 4 h, the intracellular GOx amount in IRG@RC was 0.32 $\pm$ 0.02, 0.45 $\pm$ 0.02, or 0.55 $\pm$ 0.01 pg/cell respectively (Fig. 3 d). Considering host cell viability and dosing, the therapeutic macrophage express was constructed with GNPs at 2.5 μg/mL for 2 h. CLSM images in Fig. S5 displayed that the distribution of IR (red fluorescence) and GNPs (green fluorescence) in cytoplasm with normal cell morphology.

The photothermal conversion ability affected photothermal ablation-

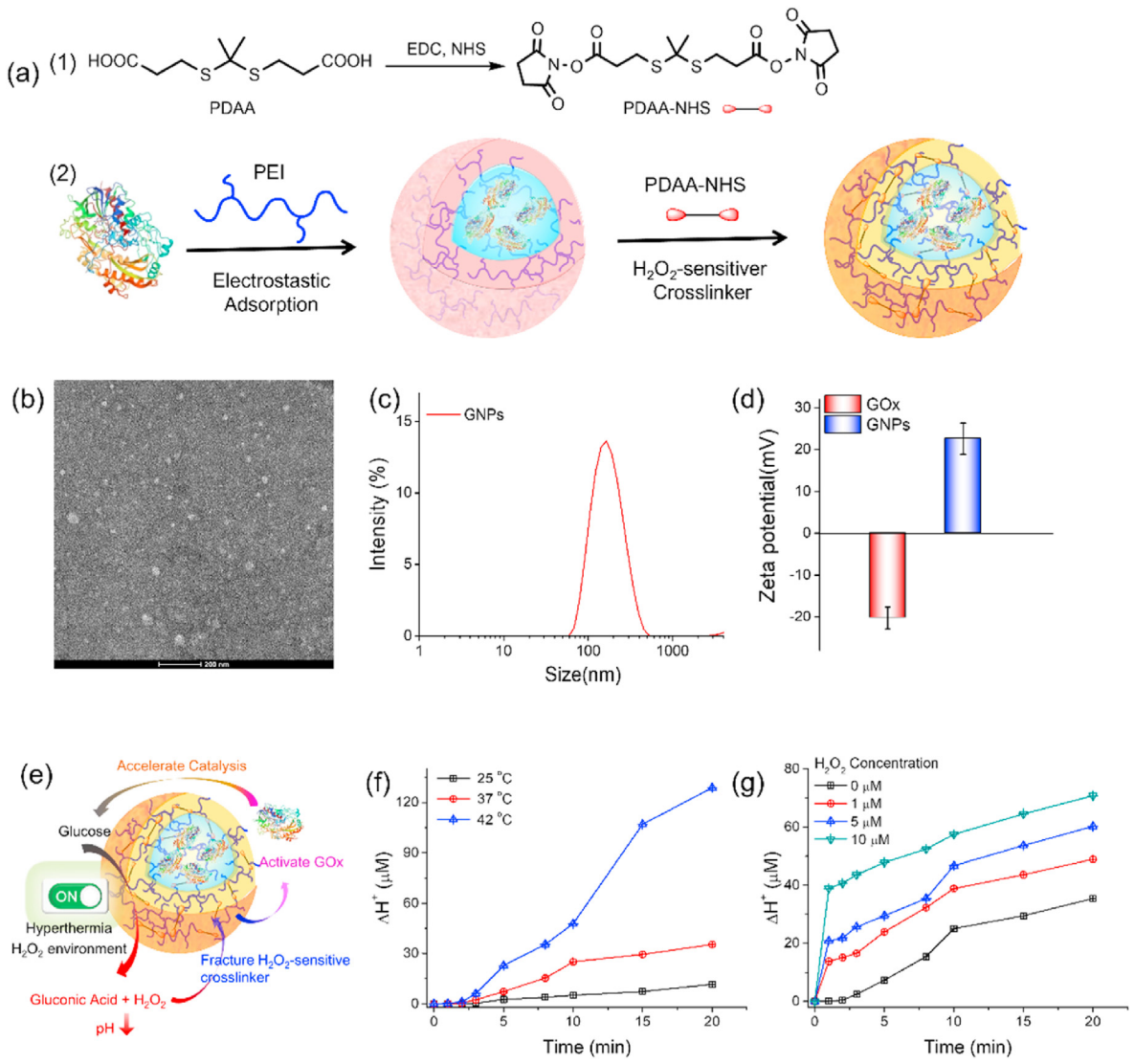

Fig. 2. Fabrication and characterization of GNPs. (a) Schematic illustration of the GNPs: (1) activation step of H_2O_2-sensitive crosslinker PDAA, and (2) the fabrication process of GNPs. (b) TEM image. (c) Hydrodynamic size and (d) zeta potential of GNPs. (e) Schematic illustration of the catalytic activity of GNPs. The H^+ concentration change (ΔH^+) of GNPs (f) in different H_2O_2 concentration and (g) different temperature.

induced release and catalytic activity of the encapsulated GNPs. As illustrated in *in vitro* thermal images (Fig. 3e), the temperature of the therapeutic macrophage expresses (IR@RC and IRG@RC) increased rapidly with laser irradiation time. The temperature raised from room temperature to 40 °C in the first 1 min, and then the temperature continued to increase, reaching 47 °C after 5 min irradiation (Fig. 3f). These efficient photothermal ablation of therapeutic expresses could ensure the release of laden GNPs with enhanced catalytic activity for effective tumor photothermal-amplified starvation therapy. CLSM images in Fig. S5 displayed the photothermal ablation of IRG@RC. After laser irradiation, the cell membrane of macrophage expresses is completely shrunken, and membrane fragments (red circles) with green fluorescence could be observed, indicating the release of GNPs from the host cells. In following, the fluorescence imaging capability of the therapeutic expresses was monitored to evaluate their application potential for fluorescent imaging navigation. As depicted in Fig. 3g, the strong fluorescence signal could be observed in both IR@RC and IRG@RC, suggesting the non-destructive fluorescence property with GNPs package. In addition, the fluorescent signal intensity after laser irradiation demonstrated the potential for imaging after PTT.

3.3. IRG@RC expresses mediated the intracellular environment of tumor

The prerequisite for IRG@RC expresses to initiate tumor starvation therapy is that the packaged GNPs were released from host express and transferred to the interior of tumor cells. The drug efflux behavior (Fig. 4a) illustrated the time-dependent and laser-responsive increase of GNPs in the supernatant. Of note, the released GNPs amount was ~9% in the first 12 h, while it increased to ~20% with the immediately exposed to laser. At final ~60% of the packaged GNPs was released in 60 h, and the released GNPs amount reached ~90% with laser irradiation. Previous studies have shown that it only takes 6–12 h for macrophages to migrate to tumors by intravenous injection [40,41]. Therefore, macrophage expresses could ensure effective delivery of drugs into the tumor. Combined the cell viability data in Fig. 3b, IRG@RC expresses could maintain its viability and precise delivery of GNPs. Subsequently, the transfer behavior of GNPs between expresses and tumor cells were tracked by confocal laser microscope (Fig. 4b). The red fluorescence referred to IR-820 still located in the cytoplasm of the host expresses, while the green fluorescence of the rhodamine-labelled GNPs migrated into 4T1 tumor cells, and the green fluorescence intensity in tumor cells were enhanced with laser irradiation. The fluorescence transfers revealed

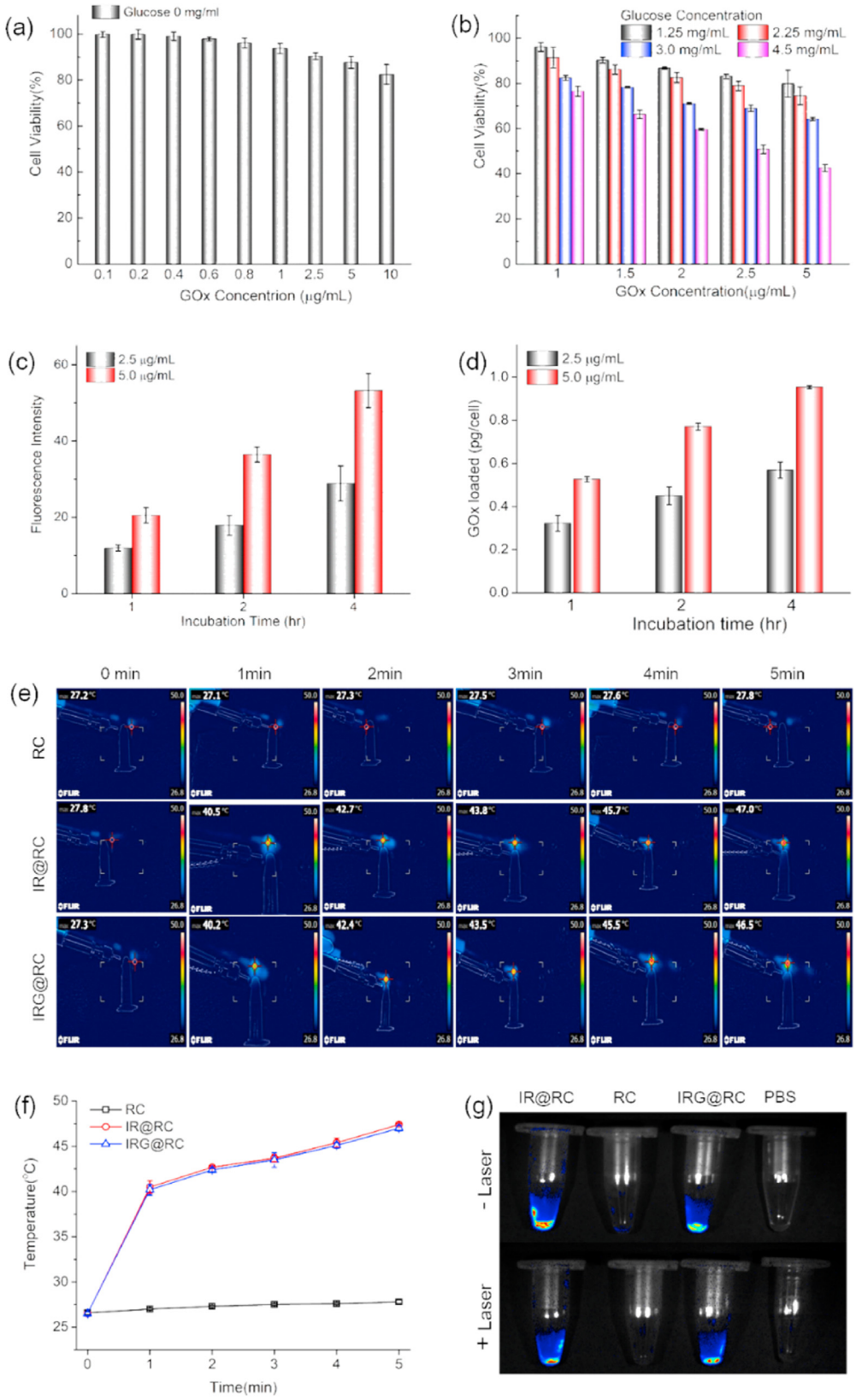

Fig. 3. Preparation and characterization of therapeutic macrophage expresses. (a) Cell viability of macrophages incubated with GNPs in glucose-free medium for different concentration by MTS assay. (b) Cell vitality of GNPs@RC expresses in medium with different glucose concentration by MTS assay. The GNPs encapsulation efficacy in macrophage expresses: (c) Intracellular fluorescence intensity of rhodamine-labelled GNPs tested by flow cytometry. (d) Intracellular amount of rhodamine-labelled GNPs analyzed by fluorescence spectra. (e) *In vitro* thermal imaging and (f) quantitative analysis of IR@RC and IRG@RC expresses with laser irradiation for a period of time. (g) *Ex vivo* fluorescence images of RC, IR@RC, and IRG@RC with/without laser irradiation.

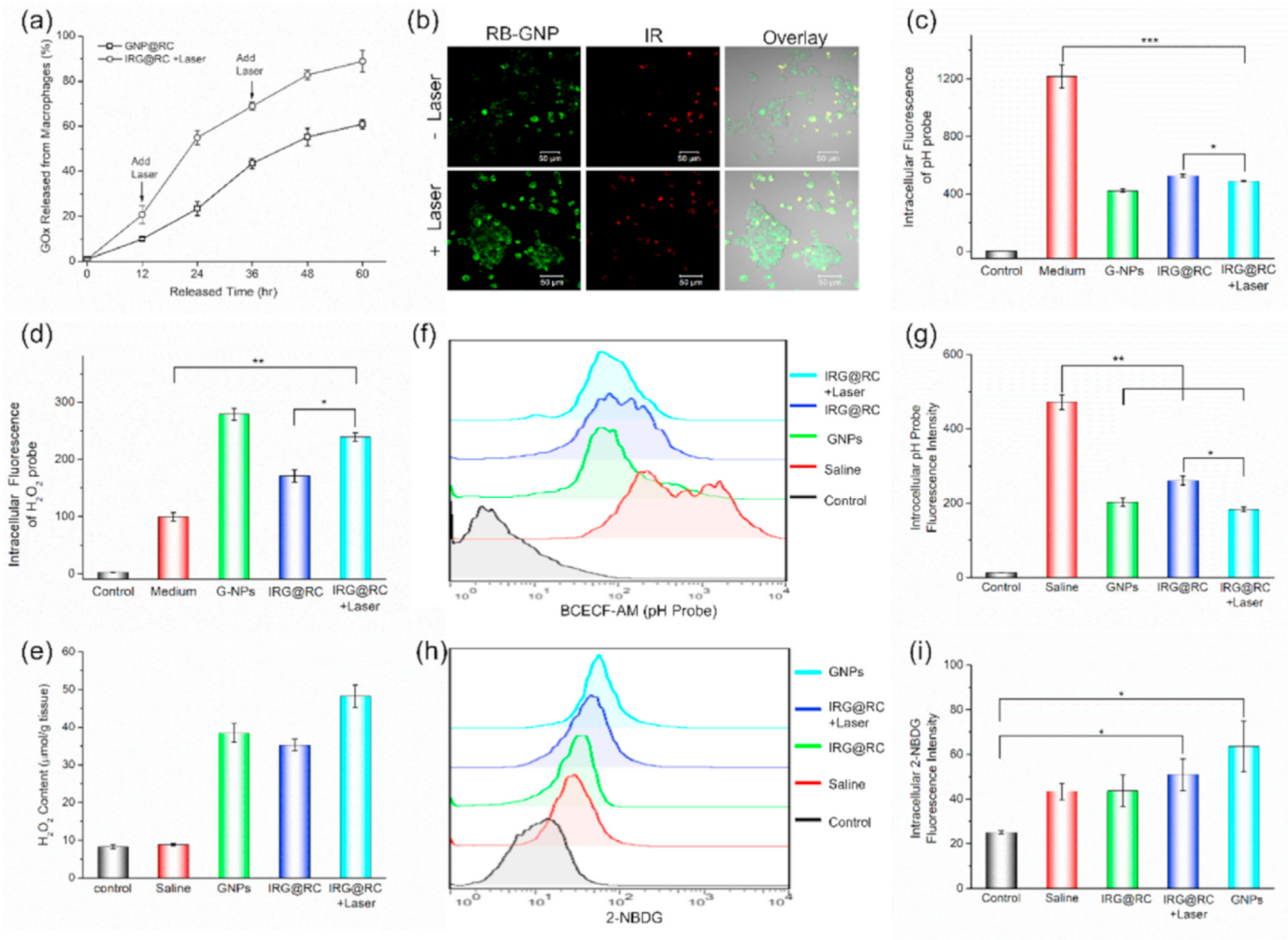

Fig. 4. The IRG@RC expresses mediated the intracellular environment of tumor. (a) Percent of released rhodamine-labelled GNPs from therapeutic expresses. (b) CLSM images of 4T1 cells co-incubated with IRG@RC express for 24 h. Flow cytometry analysis of intracellular (c) pH or (d) H_2O_2 in 4T1 cells cultured with different expresses. *In vivo* experiments: (e) H_2O_2 content at tumor tissue determine by H_2O_2 detection kit. Flow cytometry images (f and h) and intracellular fluorescence intensity (g and i) of pH probe BCECF-AM (f and g) or 2-NBDG (h and i) to determine cellular pH value and glucose consumption.

delivery process between expresses and tumor cells, illustrating the NIR laser-responsive release and photothermal accelerated delivery of GNPs.

To uncover the *in vitro* antitumor mechanism of IRG@RC expresses, the intracellular pH and H_2O_2 of 4T1 cells were assessed to examine the catalytic reaction triggered by GNPs transferred from host expresses into 4T1 cells. As detected by the pH probe (Fig. 4c and S6), 4T1 cells treated with therapeutic expresses IRG@RC presented the remarkably weakened intracellular fluorescence compared to untreated cells (Medium), indicating that a decrease in pH was induced by the released GNPs. The intracellular fluorescence was further decreased with laser-treated IRG@RC express, suggesting the laser-triggered release and photothermal-enhanced catalytic activity of GNPs. Subsequently, the intracellular H_2O_2 generation was determined by the H_2O_2 probe, BES–H_2O_2–Ac (Fig. 4d and S7). Compared with untreated cells, the intracellular H_2O_2 probe fluorescence was remarkably enhanced in cells treated with IRG@RC, and then further increased with laser irradiation. The decrease of intracellular pH and increase of H_2O_2 amount in tumor cells suggested the successful transfer of GNPs from host expresses into tumor cells to exert their catalytic capacity. It was worth noting that the laser irradiation presented a positive effect on intracellular pH and H_2O_2 level, signified that the starvation therapy could be enhanced with PTT. The NIR laser firstly triggered the selective release of packaged GNPs by photothermal ablation, inducing the photothermal accelerated convey of GNPs to tumor cells. Then the catalytic activity of GNPs was elevated by PTT-induce hyperthermia, in company with significant pH reduction and H_2O_2 production, resulting in considerable cell inhibition. The tumor microenvironment alternation induced by therapeutic expresses treatment was further studied *in vivo*. After 24 h intratumor injection, the H_2O_2 content in tumor tissue from the therapeutic expresses was significantly elevated compared to saline group (Fig. 4e). More H_2O_2 was generated in laser-treated IRG@RC express group, identifying the laser-triggered release and hyperthermia enhanced activation of GNPs. Meanwhile, the therapeutic agents treated groups induced the decrease of intracellular pH value compared to control group as indicated by the decrease green fluorescence, which was attributed to the generation of H_2O_2 and glutamic acid (Fig. 4f and g). Interestingly, the weakest intracellular green fluorescence intensity demonstrated the lowest intracellular pH value in the laser-treated IRG@RC express group. Furthermore, the consumption of glucose was evaluated with 2-NBDG indicator, which could accumulate preferentially in malignant cells to monitor the glucose uptake (Fig. 4 h and i). Compared to saline group, IRG@RC plus laser treated group displayed stronger cellular green fluorescence, indicating the excess uptake of 2-NBDG to compensate glucose depletion. Overall, these data demonstrated that IRG@RC express triggered by external laser could release and activate the packaged GNPs, which depleted the glucose to generate H_2O_2 and gluconic acid for

pH reduction. In addition, the generated H_2O_2 could in turn disrupt the H_2O_2-responsive GNPs, further activate the catalytic process. The host IRG@RC expresses owned the laser-controlled PTT-amplified starvation therapy, which would exhibit the synergistic effects on tumor treatment.

3.4. *In vitro* effect of therapeutic expresses against 4T1 cells

The therapeutic potential of the therapeutic expresses was further evaluated. FITC-tagged 4T1 cells were co-culture with therapeutic expresses with laser irradiation. As shown in Fig. 5a, the death rate was

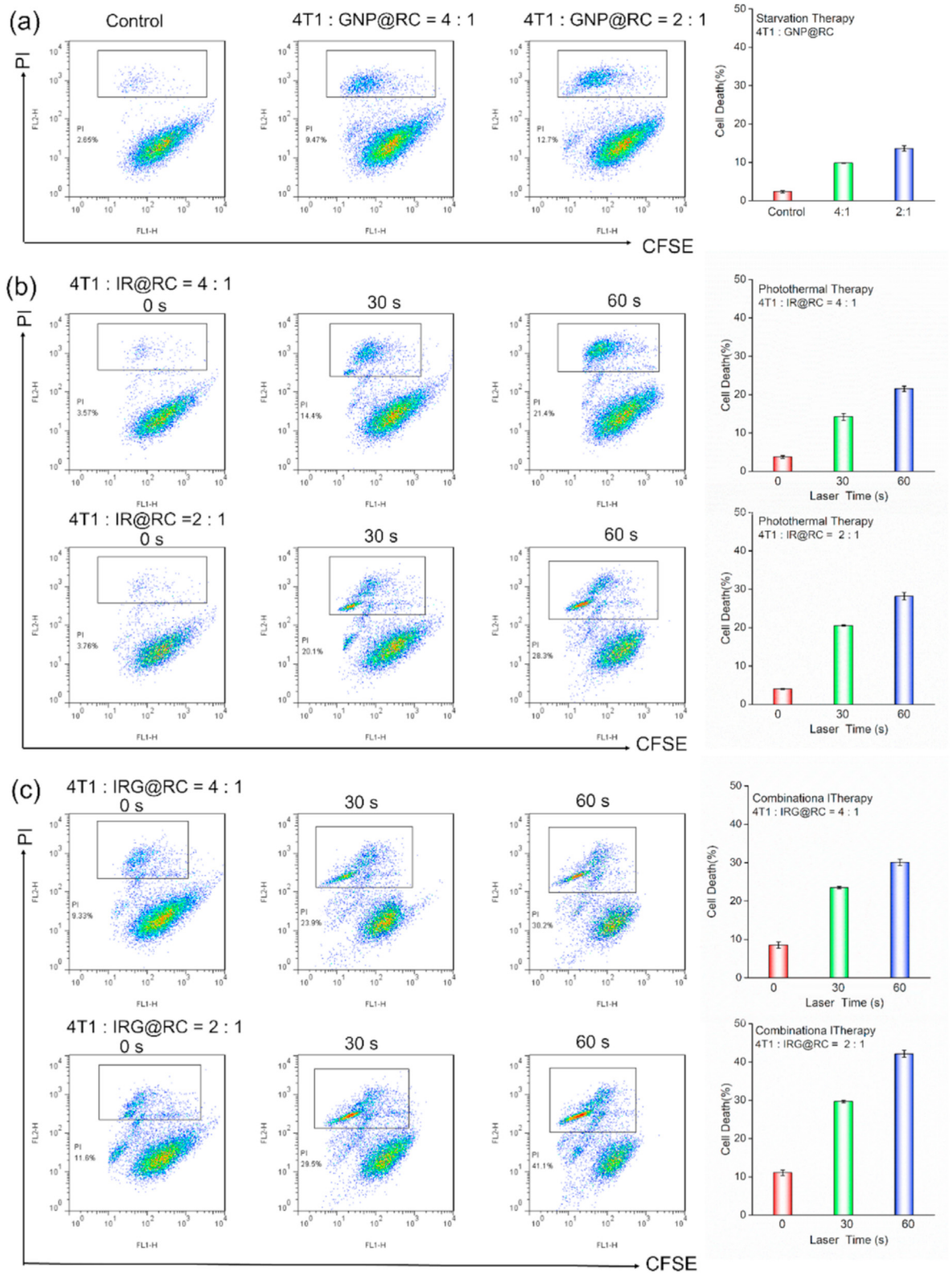

Fig. 5. *In vitro* effect of therapeutic host expresses against 4T1 cells. Cell death rate of 4T1 cells co-incubated with (a) GNP@RC, (b) IR@RC, and (c) IRG@RC with or without laser irradiation, the death percent was evaluated by flow cytometry with count of PI-sustained tumor cells.

increased with the number of the GNP@RC expresses, suggesting the effective starvation therapy of tumor cells. In photothermal therapy group with IR@RC express (Fig. 5b), the cell death rate was apparent increased with laser irradiation time. Notably, the combinational photothermal-starvation therapy groups with IRG@RC expresses (Fig. 5c) demonstrated the highest rate of death cells. The additional increase in cancer cell death was the laser-triggered rapid release of packaged GNPs and hyperthermia-enhanced catalytic activity of GOx. In brief, the PTT could accelerate the release of GNPs into tumor cells, and then GNPs was activated by intracellular high H_2O_2 levels to achieve tumor starvation treatment. It is noting that the generated H_2O_2 in CST and PTT-induced hyperthermia could in turn accelerate the activation process of GNPs to form a positive cycle, inducing PTT-amplified starvation therapy of cell apoptosis.

3.5. Imaging-guided tumor tropic migration and photothermal imaging of therapeutic expresses

As a delivery system, the targeted convey of therapeutic agents to tumor site was essential to achieve efficient tumor treatment. Macrophage and macrophage-derived cell membrane display the tumor-targeting ability as drug carriers [42]. Interestingly, the macrophage carriers not only target deliver drugs to tumor sites, but also enhance anti-tumor effects with the secretion of pro-inflammatory cytokines, while some membrane proteins during membrane extraction may lose during the extraction process, inducing the weaker targeting ability [42]. Macrophage could naturally be recruited into tumor site, however, the tumor migration property may be affected by encapsulation of therapeutic agents. With 4T1 tumor cells as lure, the migration of the FITC-F4/80 antibody labelled therapeutic expresses was tested by transwell assay. The fluorescence images (Fig. S8) displayed apparent green fluorescence, illustrating the successful migration of expresses. Subsequently, the migratory capacity of different therapeutic expresses was quantitatively analyzed by flow cytometry (Fig. 6a and S9). Compared to macrophage group (RC), the ratio of IR@RC expresses was slightly reduced, while the IRG@RC expresses demonstrated the lowest ratio. These data indicated that the package of therapeutic agents decreased the migration ability of the host expresses. However, acceptable tumor tropic movement ability still remained for tumor target.

The accurate tumor target of the IR-decorated macrophages has been explored by *ex vivo* fluorescence images and flow cytometry in our previous paper [16]. IR@RC could be successfully recruited into tumors to perform as a tumor targeted delivery tool. In this paper, encapsulated in macrophage express, the GNPs nanozymes could be protected during the blood circulation, and efficiently tumor target also achieved due to the inherent tumor tropism of macrophages. The tumor accumulation of therapeutic expresses *in vivo* was further studied by fluorescence imaging. Before animal experiments, a hemolysis test was performed to verify the biocompatibility of the therapeutic expresses (Fig. 6b and S10). No apparent hemolysis phenomena could be observed and the hemolysis rate of all samples was lower than 5%, suggesting the excellent hemocompatibility and suitability for intravenous injection. During blood circulation, the glucose can easily diffuse into macrophages to trigger the dissembling of GNPs, which maybe lead to the reduction of macrophage viability, while the targeted delivery efficiency of macrophage express cannot be particularly affected for the rapid recruitment within 6–12 h [40].

Then, the accumulated IR fluorescence within tumor was examined after intravenous injection with IR-labelled GNPs, IR@RC or IRG@RC respectively (Fig. 6c). The intense fluorescence in tumor site indicated the effective tumor targeting of IR@RC and IRG@RC. While, the column graph in Fig. S11 illustrated the fluorescence signal from the nanozymes (IR-GNPs) group was more intense than those from the therapeutic expresses (IR@RC or IRG@RC) groups, which could be attributed to the different delivery ways of tumor taken particle or cell-based expresses. Compared with normal tissues, solid tumor with abnormal tumor vessels with enlarged endothelial junction displayed enhanced permeability and retention (EPR) effect to accumulate the particles ranging in nano scale, so the circulating nanozymes could significantly aggregate at tumor sites in short term [43,44]. The macrophage-based express was recruited into tumor site by the pertinent chemo attractant and growth factors, which was relatively slow as compared to EPR. Notably, compared to nanozymes, therapeutic expresses could detain in tumor tissue for a long time. As displayed in Fig. 6 c and d, ~50% of fluorescence from the IRG@RC expresses group was remained, while that in IR-labelled GNPs was ~20%. When exposed to external laser, the fluorescence signal decayed at an accelerated rate owing to the disruption of expresses, and about 35% of the signal could be detected in therapeutic expresses groups after 6 day. Nanoparticles based delivery system faces the inherent restriction of small size and easy removal from tumors. The tumor-aggregated macrophages expresses are polarized by factors released from cancer cells within the tumor microenvironment (TME) and take part in the tumor progresses, reducing the risk of blood reflux and prolonging tumor retention.

For a photothermal cell-based delivery system, the *in vivo* photothermal conversion capability should be evaluated to assess the potential for tumor PTT. Given the excellent photothermal conversion *in vitro* and efficient tumor target property *in vivo*, the extraordinary photothermal heating in tumor site was recorded in real-time (Fig. 6 e and f). The local temperature in tumor site increased significantly with irradiation time, and the final temperature was up to 48 °C after irradiated for 5 min. The rapid increased temperature was enough to destroy the expresses to release the packaged drugs and kill the neighboring tumor cells. The detained IRG@RC expresses at tumor site demonstrated the well photothermal conversion to 808 nm laser, spatiotemporally achieving photo-triggered unpackage of GNPs. Additionally, the host expresses that detained at the tumor site for a long time reduced the frequency of administration to achieve well therapeutic effect.

3.6. Combinational photothermal and starvation therapy on tumor in vivo

In light of the strong performance by IRG@RC expresses in the upper experiments, the *in vivo* therapeutic efficacy of IRG@RC expresses was evaluated in 4T1-Luc bearing mice. The interval and cycle of intravenous administration was determined according to the remained fluorescence signal in tumor site. Mice were injected weekly with PBS, IR-GNPs, and therapeutic expresses, respectively, followed by 808 nm laser irradiation at day 1 and day 4 after injection (Fig. 7a). The tumor volume and fluorescence signal intensity in bioluminescence imaging were recorded to assess the tumor development (Fig. 7 b, c and d). Compared to the rapid development of tumors in the saline group, the tumor proliferation was inhibited in the therapeutic groups. Notably, the tumor inhibition was ameliorated in the therapeutic expresses (IR@RC or IRG@RC) groups compared with the nanozyme group (IR-GNPs), mainly due to the preferential accumulation and long-time retention in tumor site. In the IRG@RC express plus laser group, tumor proliferation was effectively inhibited due to synergism of photothermal-amplified starvation modalities leading to an almost complete inhibition of tumor development. Consistent with the above tumor inhibition data, the qualitative analysis displayed a 4-fold reduction in tumor weight for the IRG@RC express plus laser group as compared to the saline group (Fig. 7 e and f). These results illustrated that the combinational photothermal and starvation therapy in the therapeutic expresses (IRG@RC) could lead to a synergistic effect on tumor treatment. The body weight curve in Fig. 7g demonstrated no significant decline in body weight in comparison to the saline group, indicating the low systematic toxicity of the therapeutic cells.

At the end of the treatment, the tumors were collected for histological and immunofluorescence analyses (Fig. 7h). H&E staining revealed noticeable damage to tumor cells in the IRG@RC expresses plus laser group by the observed nuclear condensation and cell shrinkage. Furthermore, the evident inhibited proliferation and significant severer

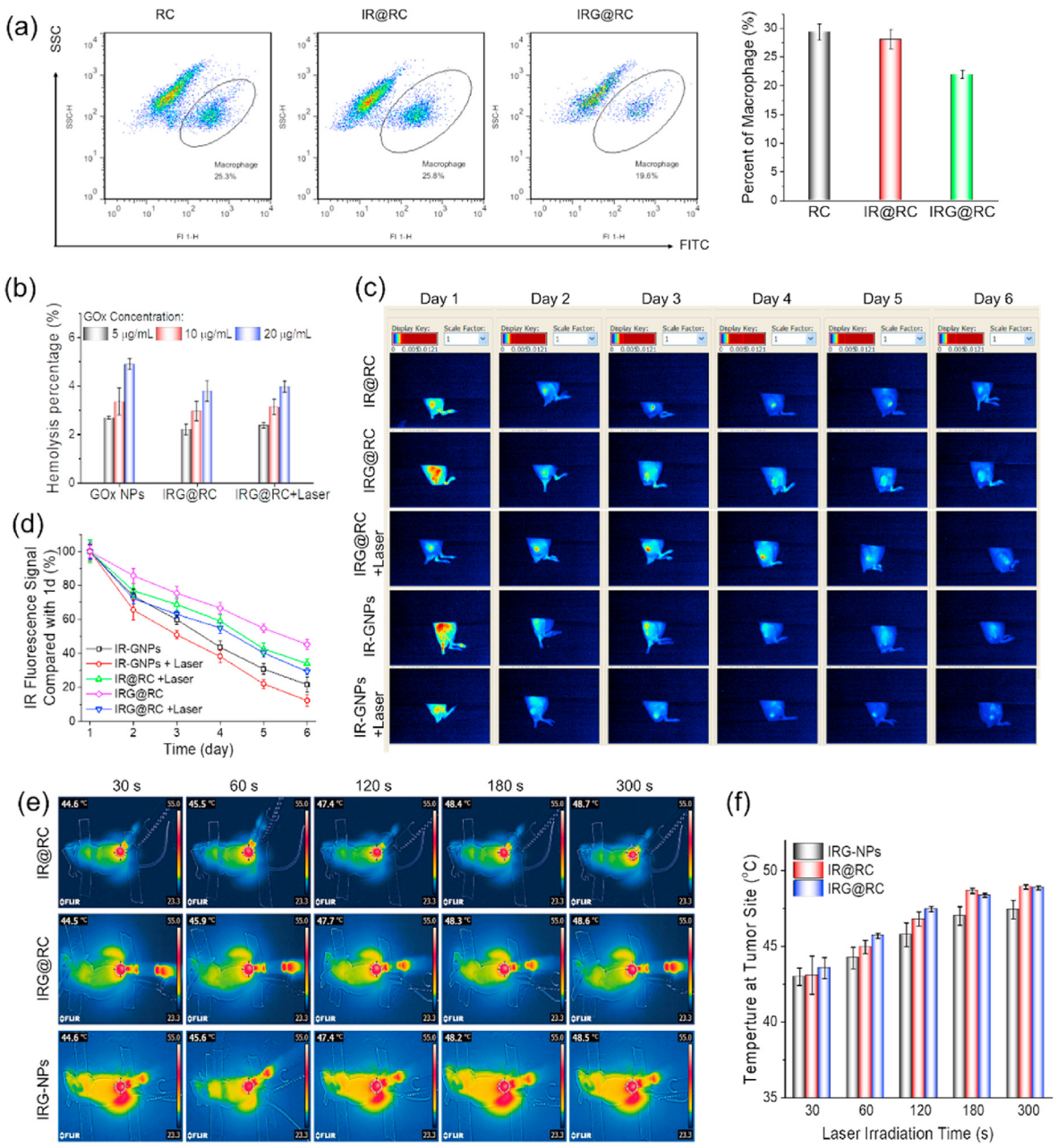

Fig. 6. Imaging-guided tumor tropic migration and photothermal imaging of therapeutic expresses. (a) Flow cytometry images and the relative quantitative analysis of rate of expresses number in bottom chamber. (b) Hemolysis analysis of therapeutic agents. (c) *In vivo* fluorescence images of tumor-bearing mice after receiving intravenous injection of kinds of therapeutic agents for different times, and (d) the relative quantitative analysis of the fluorescence signal in tumor. Thermal imaging at tumor site with laser irradiation, (e) *In vivo* infrared thermography and (f) relative analysis.

apoptosis of tumor cells were observed in IRG@RC plus laser group from Ki67, PCNA and TUNEL staining respectively. These data were in accordance with the therapeutic outcome of i*n vivo* antitumor experiment.

4. Conclusion

In summary, a nanozyme-laden intelligent macrophages express based on IR820-macrophage loaded with GOx nanoparticles was successfully constructed for tumor synergetic photothermal-activated starvation therapy. H_2O_2-responsive GOx nanozyme shielded enzyme activity to maintain the host express viability for tumor targeting. The photosensitizer IR laden in IRG@RC achieved the dual function of PTT and fluorescence imaging. With fluorescence navigation, the imaging-guided precise delivery was achieved due to the inherent tumor tropism of macrophages-based express. In addition, the tumor local unpackage of the laden therapeutic agents was triggered by the external laser and special TME simulation. With imaging guidance, external laser-triggered PTT fractured the expresses to release the packed GNPs, which then activated with the high H_2O_2 level in tumor microenvironment to start the starvation therapy. The mild temperature from PTT and the GNPs catalyzed H_2O_2 generation further induced GNPs activation to enhance the starvation therapy. Thus, IRG@RC express exerted multi-functions as laser-induce drug release and activation, tumor microenvironment-responsive, and circular amplification property, achieving the synergistic effects of PTT and starvation therapy *in vitro* and *in vivo*. In brief, the functional therapeutic macrophage-based express enabled real-time imaging, targeted drug delivery, spatiotemporal

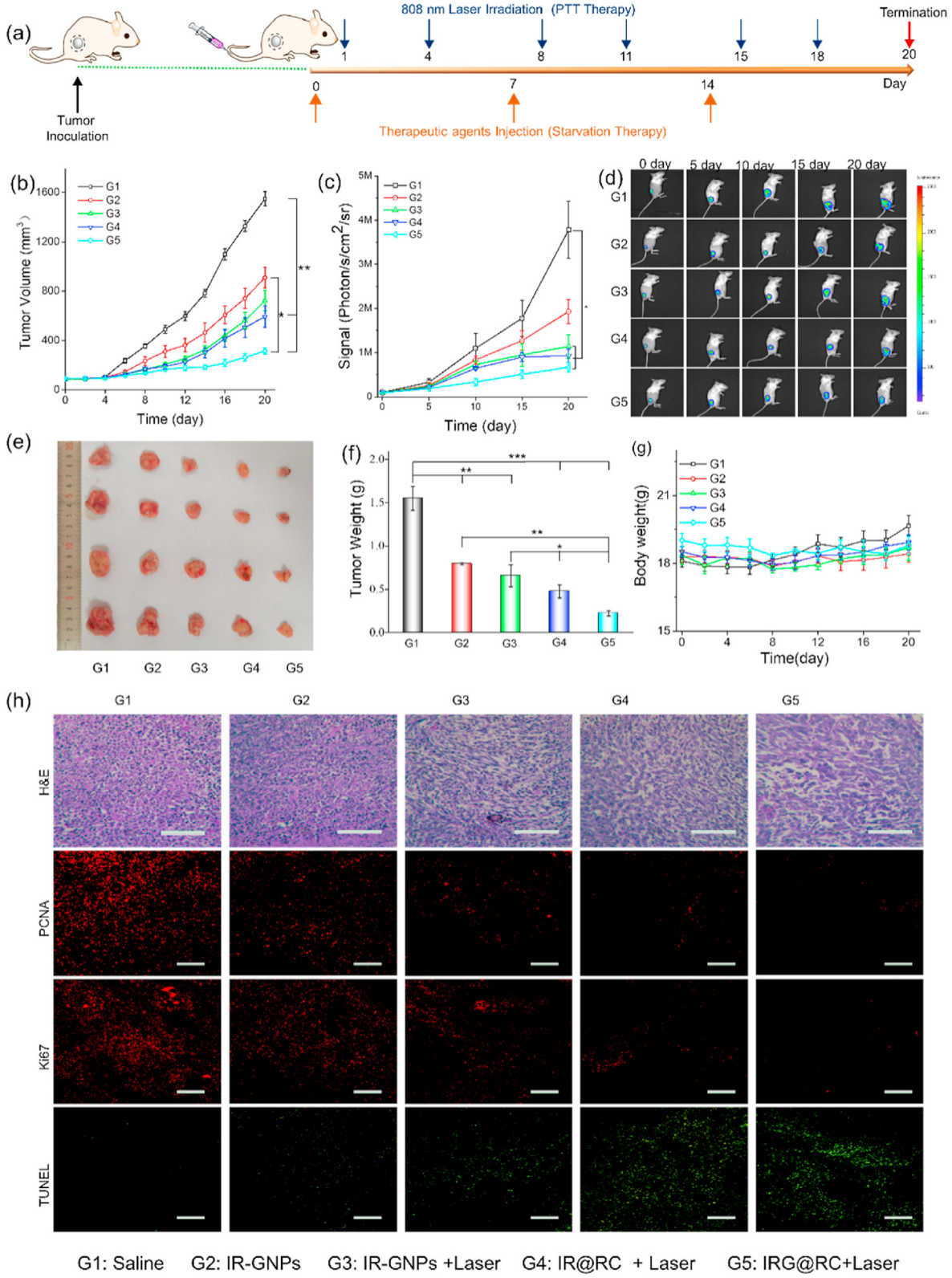

Fig. 7. Antitumor efficacy on 4T1-Luc-tumor bearing mice. (a) Protocol of combinational photothermal and starvation therapy. (b) Relative tumor volume during treatment. (c) Quantitative analysis for bioluminescence signals and (d) Representative bioluminescence images of 4T1 tumors in different groups. (e) Optical photos, and (f) the averaged tumor weight of excised tumor from the mice after 20 days of treatment. (g) Body weight curves during treatment. (h) H&E, PCNA, Ki67 and TUNEL staining images of the dissected tumor tissues after 20 days of treatment. Scale bar: 100 μm.

release and activation of nanozyme for PTT-amplified starvation therapy under fluorescence imaging guidance, distributing great potential for cancer therapy.

Credit author statement

Yan Zhang: Methodology, Formal analysis ,Investigation, Writing - Original Draft, Visualization. **Kunpeng Wang:** Investigation, Validation, Writing - Original Draft. **Guozheng Xing:** Investigation, Formal analysis. **Xia Dong:** Methodology, Writing - Review & Editing, Project administration, Funding acquisition. **Dunwan Zhu:** Resources, Funding acquisition. **Wenzhi Yang:** Conceptualization, Validation, Writing - Review & Editing, Project administration, **Lin Mei:** Resources, Project administration. **Feng Lv:** Conceptualization, Writing - Review & Editing, Supervision, Funding acquisition.

Declaration of competing interest

The authors declare that they have no known competing financial interests or personal relationships that could have appeared to influence the work reported in this paper.

Data availability

Data will be made available on request.

Acknowledgments

This work was supported by the National Natural Science Foundation of China (31870951, 81701813), the Natural Science Foundation of Tianjin, China (20JCYBJC00150, 19JCQNJC13200), the Fundamental Research Funds for the Central Universities (3332021068, 2019PT320028) and the CAMS Innovation Fund for Medical Sciences (2021-I2M-1-058).

Appendix A. Supplementary data

Supplementary data to this article can be found online at https://doi.org/10.1016/j.mtbio.2022.100421.

References

[1] I. Martínez-Reyes, N.S. Chandel, Cancer metabolism: looking forward, Nat. Rev. Cancer 21 (10) (2021) 669–680, https://doi.org/10.1038/s41568-021-00378-6.
[2] M.G. Vander Heiden, R.J. DeBerardinis, Understanding the intersections between metabolism and cancer biology, Cell 168 (4) (2017) 657–669, https://doi.org/10.1016/j.cell.2016.12.039.
[3] N.N. Pavlova, C.B. Thompson, The emerging hallmarks of cancer metabolism, Cell Metabol. 23 (1) (2016) 27–47, https://doi.org/10.1016/j.cmet.2015.12.006.
[4] C. Cao, N. Yang, Y. Su, Z. Zhang, C. Wang, X. Song, P. Chen, W. Wang, X. Dong, Starvation, ferroptosis, and prodrug therapy synergistically enabled by a cytochrome c oxidase like nanozyme, Adv. Mater. 34 (29) (2022), 2203236, https://doi.org/10.1002/adma.202203236.
[5] B. Yang, L. Ding, Y. Chen, J. Shi, Augmenting tumor-starvation therapy by cancer cell autophagy inhibition, Adv. Sci. 7 (6) (2020), 1902847, https://doi.org/10.1002/advs.201902847.
[6] W. Fan, N. Lu, P. Huang, Y. Liu, Z. Yang, S. Wang, G. Yu, Y. Liu, J. Hu, Q. He, J. Qu, T. Wang, X. Chen, Glucose-responsive sequential generation of hydrogen peroxide and nitric oxide for synergistic cancer starving-like/gas therapy, Angew. Chem. Int. Ed. 56 (5) (2017) 1229–1233, https://doi.org/10.1002/anie.201610682.
[7] F. Shao, Y. Wu, Z. Tian, S. Liu, Biomimetic nanoreactor for targeted cancer starvation therapy and cascade amplificated chemotherapy, Biomaterials 274 (2021), 120869, https://doi.org/10.1016/j.biomaterials.2021.120869.
[8] L.-H. Fu, C. Qi, J. Lin, P. Huang, Catalytic chemistry of glucose oxidase in cancer diagnosis and treatment, Chem. Soc. Rev. 47 (17) (2018) 6454–6472, https://doi.org/10.1039/C7CS00891K.
[9] L. Dai, M. Yao, Z. Fu, X. Li, X. Zheng, S. Meng, Z. Yuan, K. Cai, H. Yang, Y. Zhao, Multifunctional metal-organic framework-based nanoreactor for starvation/oxidation improved indoleamine 2,3-dioxygenase-blockade tumor immunotherapy, Nat. Commun. 13 (1) (2022) 2688, https://doi.org/10.1038/s41467-022-30436-y.
[10] X. Liu, Z. Liu, K. Dong, S. Wu, Y. Sang, T. Cui, Y. Zhou, J. Ren, X. Qu, Tumor-activatable ultrasmall nanozyme generator for enhanced penetration and deep catalytic therapy, Biomaterials 258 (2020), 120263, https://doi.org/10.1016/j.biomaterials.2020.120263.
[11] M. Huo, L. Wang, Y. Chen, J. Shi, Tumor-selective catalytic nanomedicine by nanocatalyst delivery, Nat. Commun. 8 (1) (2017) 357, https://doi.org/10.1038/s41467-017-00424-8.
[12] Z. Shi, Q. Li, L. Mei, pH-Sensitive nanoscale materials as robust drug delivery systems for cancer therapy, Chin. Chem. Lett. 31 (6) (2020) 1345–1356, https://doi.org/10.1016/j.cclet.2020.03.001.
[13] Z. Wang, Z. Li, Z. Sun, S. Wang, Z. Ali, S. Zhu, S. Liu, Q. Ren, F. Sheng, B. Wang, Y. Hou, Visualization nanozyme based on tumor microenvironment "unlocking" for intensive combination therapy of breast cancer, Sci. Adv. 6 (48) (2020), eabc8733, https://doi.org/10.1126/sciadv.abc8733.
[14] Q. Chen, L. Feng, J. Liu, W. Zhu, Z. Dong, Y. Wu, Z. Liu, Intelligent albumin–MnO2 nanoparticles as pH-/H2O2-responsive dissociable nanocarriers to modulate tumor hypoxia for effective combination therapy, Adv. Mater. 28 (33) (2016) 7129–7136, https://doi.org/10.1002/adma.201601902.
[15] Y. Zhang, Y. Sun, X. Dong, Q.-S. Wang, D. Zhu, L. Mei, H. Yan, F. Lv, A platelet intelligent vehicle with navigation for cancer photothermal-chemotherapy, ACS Nano 16 (4) (2022) 6359–6371, https://doi.org/10.1021/acsnano.2c00453.
[16] Y. Zhang, Q. Wang, T. Ma, D. Zhu, T. Liu, F. Lv, Tumor targeted combination therapy mediated by functional macrophages under fluorescence imaging guidance, J. Contr. Release 328 (2020) 127–140, https://doi.org/10.1016/j.jconrel.2020.08.052.
[17] H. Cao, H. Wang, X. He, T. Tan, H. Hu, Z. Wang, J. Wang, J. Li, Z. Zhang, Y. Li, Bioengineered macrophages can responsively transform into nanovesicles to target lung metastasis, Nano Lett. 18 (8) (2018) 4762–4770, https://doi.org/10.1021/acs.nanolett.8b01236.
[18] T. Liang, R. Zhang, X. Liu, Q. Ding, S. Wu, C. Li, Y. Lin, Y. Ye, Z. Zhong, M. Zhou, Recent advances in macrophage-mediated drug delivery systems, Int. J. Nanomed. 16 (2021) 2703–2714, https://doi.org/10.2147/IJN.S298159.
[19] Y. Zhang, Y. Zhao, Q. Li, Y. Wang, Macrophages, as a promising strategy to targeted treatment for colorectal cancer metastasis in tumor immune microenvironment, Front. Immunol. 12 (2021) 685978, https://doi.org/10.3389/fimmu.2021.685978, 685978.
[20] P. Sun, Q. Deng, L. Kang, Y. Sun, J. Ren, X. Qu, A smart nanoparticle-laden and remote-controlled self-destructive macrophage for enhanced chemo/chemodynamic synergistic therapy, ACS Nano 14 (10) (2020) 13894–13904, https://doi.org/10.1021/acsnano.0c06290.
[21] Y. Huang, Z. Guan, X. Dai, Y. Shen, Q. Wei, L. Ren, J. Jiang, Z. Xiao, Y. Jiang, D. Liu, Z. Huang, X. Xu, Y. Luo, C. Zhao, Engineered macrophages as near-infrared light activated drug vectors for chemo-photodynamic therapy of primary and bone metastatic breast cancer, Nat. Commun. 12 (1) (2021) 4310, https://doi.org/10.1038/s41467-021-24564-0.
[22] Y. Xia, L. Rao, H. Yao, Z. Wang, P. Ning, X. Chen, Engineering macrophages for cancer immunotherapy and drug delivery, Adv. Mater. 32 (40) (2020), 2002054, https://doi.org/10.1002/adma.202002054.
[23] T. Etrych, H. Lucas, O. Janoušková, P. Chytil, T. Mueller, K. Mäder, Fluorescence optical imaging in anticancer drug delivery, J. Contr. Release 226 (2016) 168–181, https://doi.org/10.1016/j.jconrel.2016.02.022.
[24] J. Kong, R. Zou, G.-L. Law, Y. Wang, Biomimetic multifunctional persistent luminescence nanoprobes for long-term near-infrared imaging and therapy of cerebral and cerebellar gliomas, Sci. Adv. 8 (10) (2022), eabm7077, https://doi.org/10.1126/sciadv.abm7077.
[25] X. Dong, A. Yang, Y. Bai, D. Kong, F. Lv, Dual fluorescence imaging-guided programmed delivery of doxorubicin and CpG nanoparticles to modulate tumor microenvironment for effective chemo-immunotherapy, Biomaterials 230 (2020) 119659, https://doi.org/10.1016/j.biomaterials.2019.119659.
[26] R. Fan, C. Chen, H. Hou, D. Chuan, M. Mu, Z. Liu, R. Liang, G. Guo, J. Xu, Tumor acidity and near-infrared light responsive dual drug delivery polydopamine-based nanoparticles for chemo-photothermal therapy, Adv. Funct. Mater. 31 (18) (2021), 2009733, https://doi.org/10.1002/adfm.202009733.
[27] X. Chen, H. Yang, X. Song, H. Liang, Y. Wei, J. Lu, M. Barz, R. Jin, Y. Nie, Integrated and dual-responsive lipopeptide nanovector with parallel effect to tumor and microenvironment regulation by efficient gene and drug co-delivery, Chin. Chem. Lett. (2022), 107753, https://doi.org/10.1016/j.cclet.2022.107753.
[28] S.H. Yun, S.J.J. Kwok, Light in diagnosis, therapy and surgery, Nat. Biomed. Eng. 1 (1) (2017), https://doi.org/10.1038/s41551-016-0008.
[29] P. Gao, H. Wang, Y. Cheng, Strategies for efficient photothermal therapy at mild temperatures: progresses and challenges, Chin. Chem. Lett. 33 (2) (2022) 575–586, https://doi.org/10.1016/j.cclet.2021.08.023.
[30] J. Zhou, M. Li, Y. Hou, Z. Luo, Q. Chen, H. Cao, R. Huo, C. Xue, L. Sutrisno, L. Hao, Y. Cao, H. Ran, L. Lu, K. Li, K. Cai, Engineering of a nanosized biocatalyst for combined tumor starvation and low-temperature photothermal therapy, ACS Nano 12 (3) (2018) 2858–2872, https://doi.org/10.1021/acsnano.8b00309.
[31] J.J. Hu, M.D. Liu, F. Gao, Y. Chen, S.Y. Peng, Z.H. Li, H. Cheng, X.Z. Zhang, Photo-controlled liquid metal nanoparticle-enzyme for starvation/photothermal therapy of tumor by win-win cooperation, Biomaterials 217 (2019) 119303, https://doi.org/10.1016/j.biomaterials.2019.119303.
[32] X. Li, J.F. Lovell, J. Yoon, X. Chen, Clinical development and potential of photothermal and photodynamic therapies for cancer, Nat. Rev. Clin. Oncol. 17 (11) (2020) 657–674, https://doi.org/10.1038/s41571-020-0410-2.
[33] Y. Zou, W. Liu, W. Sun, J. Du, J. Fan, X. Peng, Highly inoxidizable heptamethine cyanine–glucose oxidase conjugate nanoagent for combination of enhanced photothermal therapy and tumor starvation, Adv. Funct. Mater. 32 (17) (2022), 2111853, https://doi.org/10.1002/adfm.202111853.

[34] F. Tian, X. Zhong, J. Zhao, Y. Gu, Y. Fan, F. Shi, Y. Zhang, Y. Tan, W. Chen, C. Yi, M. Yang, Hybrid theranostic microbubbles for ultrasound/photoacoustic imaging guided starvation/low-temperature photothermal/hypoxia-activated synergistic cancer therapy, J. Mater. Chem. B 9 (45) (2021) 9358–9369, https://doi.org/10.1039/D1TB01735G.

[35] J. Wu, Y. Zhang, K. Jiang, X. Wang, N.T. Blum, J. Zhang, S. Jiang, J. Lin, P. Huang, Enzyme-engineered conjugated polymer nanoplatform for activatable companion diagnostics and multistage augmented synergistic therapy, Adv. Mater. 34 (18) (2022) 2200062, https://doi.org/10.1002/adma.202200062.

[36] S. Wang, R. Chen, Q. Yu, W. Huang, P. Lai, J. Tang, L. Nie, Near-infrared plasmon-boosted heat/oxygen enrichment for reversing rheumatoid arthritis with metal/semiconductor composites, ACS Appl. Mater. Interfaces 12 (41) (2020) 45796–45806, https://doi.org/10.1021/acsami.0c13261.

[37] J. Li, Z. Wei, X. Lin, D. Zheng, M. Wu, X. Liu, J. Liu, Programmable therapeutic nanodevices with circular amplification of H2O2 in the tumor microenvironment for synergistic cancer therapy, Adv. Healthc. Mater. 8 (10) (2019), 1801627, https://doi.org/10.1002/adhm.201801627.

[38] P. Pacheco, D. White, T. Sulchek, Effects of microparticle size and Fc density on macrophage phagocytosis, PLoS One 8 (4) (2013) e60989, https://doi.org/10.1371/journal.pone.0060989, e60989.

[39] J. Zibolka, A. Wolf, L. Rieger, C. Rothgänger, A. Jörns, B. Lutz, A. Zimmer, F. Dehghani, I. Bazwinsky-Wutschke, Influence of cannabinoid receptor deficiency on parameters involved in blood glucose regulation in mice, Int. J. Mol. Sci. 21 (9) (2020) 3168, https://doi.org/10.3390/ijms21093168.

[40] W. Zhang, M. Wang, W. Tang, R. Wen, S. Zhou, C. Lee, H. Wang, W. Jiang, I.M. Delahunty, Z. Zhen, H. Chen, M. Chapman, Z. Wu, E.W. Howerth, H. Cai, Z. Li, J. Xie, Nanoparticle-laden macrophages for tumor-tropic drug delivery, Adv. Mater. 30 (50) (2018), 1805557, https://doi.org/10.1002/adma.201805557.

[41] J. Si, S. Shao, Y. Shen, K. Wang, Macrophages as active nanocarriers for targeted early and adjuvant cancer chemotherapy, Small 12 (37) (2016) 5108–5119, https://doi.org/10.1002/smll.201601282.

[42] Y. Xia, L. Rao, H. Yao, Z. Wang, P. Ning, X. Chen, Engineering macrophages for cancer immunotherapy and drug delivery, advanced materials 32 (40) (2020), e2002054, https://doi.org/10.1002/adma.202002054 deerfield beach, fla.

[43] E. Blanco, H. Shen, M. Ferrari, Principles of nanoparticle design for overcoming biological barriers to drug delivery, Nat. Biotechnol. 33 (9) (2015) 941–951, https://doi.org/10.1038/nbt.3330.

[44] M.T. Manzari, Y. Shamay, H. Kiguchi, N. Rosen, M. Scaltriti, D.A. Heller, Targeted drug delivery strategies for precision medicines, Nat. Rev. Mater. 6 (4) (2021) 351–370, https://doi.org/10.1038/s41578-020-00269-6.